Vol. 23, No. 3(2024) Mat24245
Revista Mexicana de Ingeniería Química

Study on wild grasses as a potential source of cellulose nanofibers

Estudio de pastos silvestres como potencial fuente de nanofibras de celulosa

R. Herrera-Basurto[1,5*], E. Ramos-López[2], A. Rodríguez-López[2], J.C. González-Olvera[2], J. Morales-Hernández[3], A. Hurtado-Macías[4], H.J. Vergara-Hernández[5], F. Mercader-Trejo[2*]

[1] *Total Metrology in Chemistry, Dirección de Innovación y Negocios, Santiago Apóstol 128, Villas de Santiago, 76148 Santiago de Querétaro, México.*

[2] *Universidad Politécnica de Santa Rosa Jáuregui, Carr. Federal 57 QRO-SLP km 31-150, 76220, Santa Rosa Jáuregui, Santiago de Querétaro, México.*

[3] *Centro de Investigación y Desarrollo Tecnológico en Electroquímica S.C., Parque Tecnológico Querétaro s/n, Sanfandila, 76703, Pedro Escobedo, Querétaro, México.*

[4] *Centro de Investigación en Materiales Avanzados S.C, 31136, Chihuahua, México.*

[5] *Tecnológico Nacional de México, campus Morelia, Depto. Posgrado e Investigación, 58120, Morelia, México.*

Received: January 18, 2024; Accepted: May 29, 2024

Abstract

A manufacturing process is described for obtaining cellulose nanofibers from pink weed (Rhynchelytrum repens) and foxtail (Bothriochloa laguroides) plants by physicochemical methods. These plants are considered weeds since they are discarded because they have no use as livestock feed, and both have minimal biotechnological utility. The physical-chemical characterization of the nanocellulose obtained from these sources were evaluated by infrared spectrometry, thermography, microscopy characterization, dynamic light scattering, and X-ray diffraction. The cellulose nanofibers from pink grass have a length of 1-10 μm and a diameter of 30-120 nm, similar to those previously reported from different plant sources. In the case of foxtail plants, fractal feature nano-objects with lengths less than 1.5 μm, and diameters in the 20-190 nm range were obtained. Notably, this geometry for cellulose nano-objects has not been reported previously. In addition, the crystallinity index was evaluated, obtaining values of 60% for both plants, and the crystal size was estimated using the Sherrer equation.

Keywords: Cellulose nanofibers, weedy plants, fractal structure.

Resumen

Se describe un proceso de manufactura para obtener nanofibras de celulosa a partir de las plantas pasto rosado (Rhynchelytrum repens) y cola de zorra (Bothriochloa laguroides) por métodos fisicoquímicos. Estas plantas son consideradas como maleza ya que son desechadas debido a que no tienen uso como alimento de ganado, y ambas tienen utilidad biotecnológica mínima. La caracterización físico-química de la nanocelulosa obtenida por estas fuentes fue evaluada por espectrofotometría de infrarrojo, termografía, caracterización microscópica, dispersión dinámica de luz y difracción de rayos-X. Las nanofibras de celulosa del pasto rosado tienen una longitud de 1-10 μm y un diámetro de 30-120 nm, similares a las reportadas previamente de diferentes fuentes vegetales. En este caso, las plantas cola de zorra, se obtuvieron características fractales de los nano-objetos con longitudes menores que 1.5 μm y diámetros en el rango de 20-190 nm. Notablemente, esta geometría para nano-objetos de celulosa no ha sido reportada previamente. Adicionalmente, el índice de cristalinidad fue evaluado, obteniendo valores de 60% para ambas plantas, y el tamaño del cristal fue estimado utilizando la ecuación Sherrer.

Palabras clave: Nanofibras de celulosa, plantas de maleza, estructura fractal.

* *Corresponding author. E-mail*: fmercader@upsrj.edu.mx, raul.herrera@tmicnet.com;
https://doi.org/10.24275/rmiq/Mat24245
ISSN:1665-2738, *issn-e*: 2395-8472

1 Introduction

Cellulose is the most abundant organic compound in nature because it is the fundamental component of the outer cell wall of plant cells found in trees (wood) and other plants This biopolymer has also been found in algae, shrubs, and even in marine animals (French it et al., 2002). Usually, this polysaccharide is combined with other biomolecules such as lignin, hemicelluloses (Ponce it et al., 2014) (shorter carbohydrates, mainly pentosans), pectins, and fatty acids. More than 90% of cellulose production is obtained from wood, and the remaining 10% from other plants (Ioelovich, 2008). Being such an abundant polymer in nature and considering the numerous sources from which it can be obtained, cellulose has become an attractive investment market. It was valued at $297 million dollars in 2020 and is projected to reach a value of $783 million dollars by 2025, with the highest growth in Europe and North America. Currently, this market represents around 7.5 million tons per year, and cellulose is considered a high-engineering-value product that is cheap, self-sustaining, ecological, and renewable (Ltd, 2023).

Seven cellulose polymorphs are known (I_α, I_β, II, III_I, III_{II}, IV_I, IV_{II}), but only the I_α and I_β forms of cellulose are found in nature (French it et al., 2002), (Fleming it et al., 2001; Gardner & Blackwell, 2001; Marchessault, 1962). The I_α form is found predominantly in the cell walls of algae and bacteria, while the I_β form is abundant in cotton and wood. I_α and I_β celluloses can be simultaneously found in the same microfiber (Finch, 1985). On the other hand, nanocellulose, which is the minimum scaffold (individual cellulose molecules) of cellulose (Nair it et al., 2014), has been considered an innovative nanomaterial, which has positively impacted the productive sector, e.g., additive for the polymer industry (Trache it et al., 2014), reinforcing material in the development of composite materials with better mechanical properties, and the biomedical industry used as a carrier for specific drugs or platform for organic sensors, due to its high biocompatibility and biodegradation properties (Thomas it et al., 2020; Chirayil it et al., 2014; Khalid it et al., 2021; Ruiz-Palomero it et al., 2017; Bolio-López it et al., 2011; Garzón it et al., 2009).

Nanocellulose is obtained by transforming cellulose using different processes (chemical, physical, or biological or a combination), resulting in very different mechanical and optical properties of the product, when changing parameters even using the same methodology (Dufresne, 2013). There are also other references that lead us to be sure that there are still aspects that can be improved at synthesis methods, no matter the process selected (Shaghaleh, 2018).

The standard manufacturing physical processes to obtain nanocellulose are cryo-crushing, grinding, and high-pressure homogenizing, whereas the typical chemical process is acid hydrolysis, and biological process such as enzyme-assisted hydrolysis (Postek it et al., 2013). The selection of the nanocellulose manufacturing process is determined by the origin of the cellulose (Brinchi it et al., 2013; Habibi it et al., 2010).

Regarding cellulose nanofibers, there are several fabrication methods that have been reported, including phase separation, electrospinning, self-assembly and others (Anusiya and Jaiganesh, 2022), where properties and possible applications are different, mainly because solvents and reactive used during synthesis, which affect size, morphology, purity and stability of the material. Depending on the future use, some characteristics are more important, for example, if the nanomaterial is going to be use as reinforcement, thermal stability is very important, or, if it is going to be used at the biomedical industry, purity become more relevant (Isogai, 2020).

Even though synthesis methods have improved in recent years, there are still important issues to solve, mainly related with effective chemical pretreatments, and energy-efficiency (Djafari Petroudy et.al., 2021). In order to make this material more commercial, energy use during synthesis is one of the most important aspects to research.

In the present work, the process designed to obtain cellulose nanofibers from weedy plants is presented, as well as the results obtained by different analytical techniques to characterize their chemical and morphological properties. The evaluation of the mechanical properties of the obtained cellulose nanofibers was not considered in this work. However, when analyzing the results achieved and the studies reported in the literature, the synthesized nanomaterial has a high potential to be used for bio-nano composite applications (Chen *et al.*, 2018) as well as a reinforcement in polymeric composites (Winter *et al.*, 2017).

2 Materials and methods

2.1 Materials

2.1.1 Plants

The pink grass (*Rhynchelytrum repens* (Willd.) CE Hubb. (= *Melinis repens* (Willd.) (Zizka)) and foxtail (*Bothriochloa laguroides* (DC.) Herter) plants, used as the primary source of cellulose for this study, were obtained in the surroundings of the campus of the Universidad Politécnica de Santa Rosa Jáuregui, located in Querétaro, Mexico. Figure 1 shows the

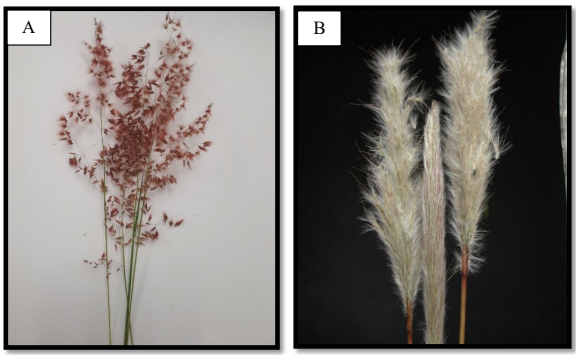

Figure 1. Images of the plants used as raw material in the study. A) Pink grass, ornamental specie commonly used in gardening, and B) Foxtail, an herbaceous plant reported as a weed in alfalfa, bean and corn.

images of the plants mentioned above.

2.1.2 Reagents

For the extraction of the fibers, the following analytical grade chemical reagents were used : type 1 water; sodium hydroxide, purity 98 %: JT Baker; denatured ethyl alcohol, purity 99.9 %: JT Baker; toluene, purity 99.9 %: JT Baker; hydrochloric acid, purity 36.5 – 38.0 %: JT Baker.

2.1.3 Laboratory Equipment and Analytical Techniques

The equipment used was the following: Terla electric oven, with a temperature range of 50 °C to 500 °C, model 60-TE-H218LDM; Sartorius water purification system, model H2OPRO-UV-Tarium pro; ADAM analytical balance, model EP 520 A, with a range of 250 g, and sensitivity of 0.0001 g; Sanyo Gallenkamp MSE disruptor, model Soniprep 150; Cole-Palmer ultrasonic bath, model EW-04711-75; TOPTION free-dryer lyophilizer, model TOPT-10B, with a minimum condenser temperature range of -50 °C, final vacuum <10 Pa; VelaQuin cooling bath, model DC-2006, with a temperature range from -20 °C to 100 °C; SEOH heating blankets, model Mantle-500, with a temperature range of 450 °C; Benchmark stirring and heating plate, model H4000-HS, with a range of temperature from 50 °C to 380 °C, and speed of 60 to 1500 rpm.

The analytical techniques used were dynamic light scattering (DLS), molecular or particle size range from 0.3 nm to 10 μm, Malvern Panalytical, Zetasizer Nano S. High-resolution scanning electron microscopy (HR-SEM), with the JEOL 7500 FE equipment. Thermogravimetric analysis was performed in a Mettler Toledo analyzer, model TGA 1. The FT-IR spectrometer used was a Thermo, model Nicolet 6700. The Transmission Electron Microscope (TEM) used was a Hitachi low vacuum, HT 7700 – EXALENS, as sample protection to observe the sample without metal coating. The X-ray diffractometer (XRD) used was a XPert-Pro, Malvern-Panalytical with Cu-Kα (λ = 1.542 Å), 30 kV and 30 mA. JADE software from The International Center for Diffraction Data, was used to identify the 2θ positions of the diffraction peaks. Scherrer equation was used to determine the crystal size from the X-Ray patterns, from foxtail and pink grass fibers. Calculations of crystal size were determined to measure the full width at half maximum intensity of peak (β) in radian located at any 2θ characteristic peak in the pattern. This means that crystal size determinations only depend on the crystal diffraction capacity and not on their morphology.

2.2 Sample preparation and analysis

2.2.1 Fiber treatment

The plants' stems were washed using water type 1 and dried in an oven at 80 °C for 24 h, then cut into sections with an approximate length of 1-2 cm. For the extraction of oil and grease content, the sections were placed in a Soxhlet system, employing a toluene/ethanol 2:1 (v/v) mixture at 90 °C for 6 h. This process was carried out in an extraction hood. Subsequently, lignin and hemicellulose were gradually removed and solubilized by a treatment of a 1 % $NaClO_2$ solution, buffered at pH 4 with 5 % w/v sodium bisulfate at 80 °C for 4 h. Afterward, the cellulose fiber was subjected to an alkaline treatment in a 3 % and 6 % NaOH solution at 80 °C to 90 °C for 2 hours for each percentage of solution. After this chemical treatment, the fibers were rinsed with water type 1 to neutralize them to a pH 7, where a white pulp was formed and finally stored in an aqueous solution.

A schematic representation of the methodology employed to obtain cellulose nanoparticles from weedy plants is shown in Figure 2.

2.2.2 Separation of cellulose nanofibers

The cellulose pulp was filtered using a vacuum pump at a force of 1 cm Hg with cellulose-acetate membrane filters (Ø 47 mm, 0.45 μm). Finally, the separated fibers were subjected to an ultrasonic homogenizer for 180 min and 440 min (See Figure 2).

2.2.3 Sample Preparation for physicochemical analysis

For FT-IR analysis, a diffuse reflectance accessory (DRIFT) was used. A sample drop was placed on the analyzer glass, and the respective spectrum was acquired. The analysis conditions were a resolution of 4 cm^{-1}, 64 scans, and a region from 4000 to 400 cm^{-1}. For thermogravimetry analysis, a portion of the obtained cellulose was placed in the corresponding sample holder for each of the analytical techniques

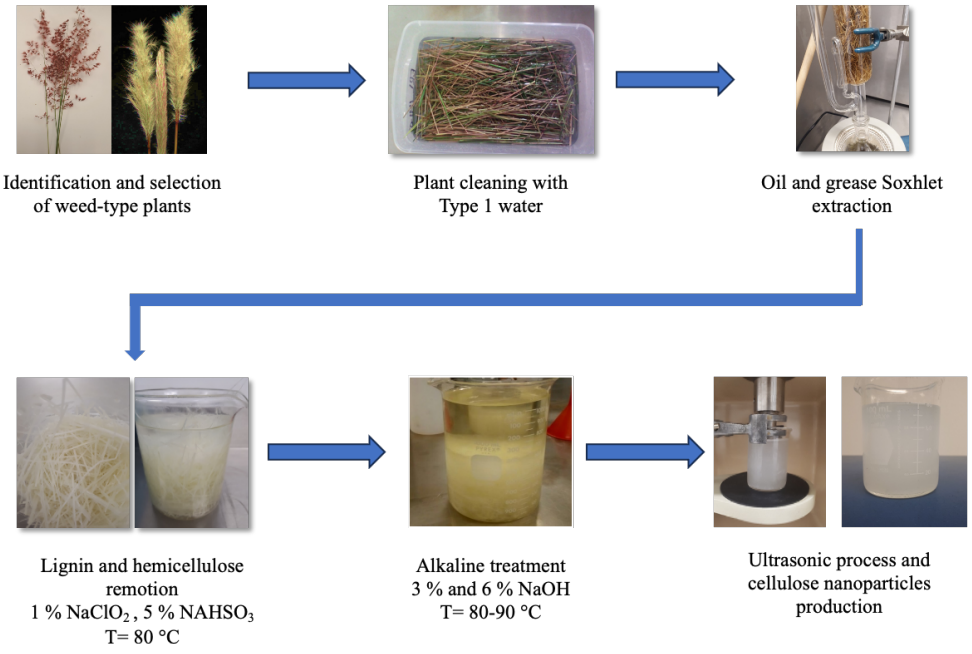

Figure 2. The process diagram to obtain cellulose nanofibers from wild plants is presented. This process involves several stages, such as removing impurities, pretreatment, and hydrolysis, to get pure and high-quality cellulose nanofibers.

used to identify the corresponding material. The thermogravimetry analysis was performed in the temperature range from 25 ºC to 750 ºC, at a rate of 10 ºC/min, in a hydrogen atmosphere, with a 50 ml/min flow.

2.2.4 *Sample Preparation for cellulose nanofibers characterization*

2.2.4.1 DLS analysis

The sample was prepared from the solution of 1 g in 100 ml, and then 30 μl of the sample was taken and deposited in a cell to add 970 μl of distilled water. Manual shaking was carried out, verifying that the optical zone of the cell had no impurities. Afterward, the cellulose nanofibers were analyzed by a Zetasizer Nano S equipment, with laser wavelength of the equipment at 632.8 nm, emitted by a helium lamp; the collection angle was 173 degrees, at a temperature of 25 °C.

2.2.4.2 HR-SEM analysis

A suspension of 1 g in 100 ml of the cellulose nanofiber solution was prepared and then sonicated for 10 min. A drop of this suspension was taken from the middle of the vial and placed on a 5 x 5 mm silicon sheet to be dried, and then HR-SEM was performed. Different fields of observation were analyzed, and images were obtained with primary and secondary electrons and X-ray analysis of the different areas.

2.2.4.3 TEM analysis

The sample for TEM analysis was taken from a cellulose nanofiber suspension sonicated for 35 min. A drop was taken from the middle of the container and placed on a carbon grid. Different fields of observation were analyzed, and bright and dark field images were obtained.

2.2.4.4 XRD analysis

The nanofiber suspension was dried for 24 h at 100 °C to obtain a solid and dry sample. The obtained powders were then placed on an amorphous glass for scanning beam measurements, ensuring the height of the sample holder did not interfere with the analysis. The X-ray beam inclined 0.7 degrees. The experimental parameters included scanning step 0.5 deg/s and measurement interval between 10 and 90 in 2 Theta grades.

3 Results

3.1 *Infrared spectrometry analysis*

Vibrational spectroscopy has been used for both qualitative and quantitative evaluation of cellulosic materials, and it has the potential to provide efficient results, using less expensive equipment (compared to XRD or NMR) for routine measurements that can be employed to determine crystalline properties and chemical composition.

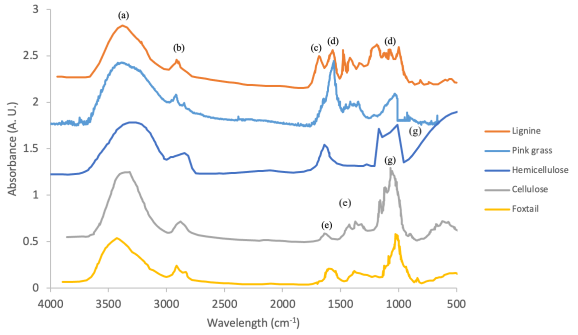

Figure 3. FTIR profiles showing the spectral fingerprint of cellulose nanomaterials obtained from weedy plants and compared whit the spectra of each nanocellulose substance.

The comparison of FT-IR results, presented in Figure 3 shows the relevant absorbance regions for the characteristic functional groups of polysaccharides under study, and for those extracted from pink grass and foxtail plants. Detailed information on absorbance wavelength and vibrational behavior of fiber components are presented in Table 1, identifying some specific absorbance peaks corresponding to lignin, hemicellulose, and cellulose. Analyzing the spectra of Figure 3, and reviewing the bibliographic information reported in Table 1, the commercial cellulose and that obtained from the foxtail plant and pink grass have characteristic absorbance in the range of 1170 - 1082 cm^{-1}, attributable to other groups at the skeletal pyranose (peak (g), Fig. 3). Moreover, the absorbance at 1640 cm^{-1} can be assigned to OH bonds with cellulose (peak (e), Fig. 3).

In the case of lignin, there are characteristic peaks in the range of 1600-1800 cm^{-1} corresponding to aromatic skeletal residues and another superimposed-on benzene (peaks (c) and (d) respectively, Fig. 3) whereas a distinguishing band is observed in the interval of . The 1765 – 1715 cm^{-1} due to C=O groups. Additionally, a peak between 3000 and 2800 cm^{-1} is formed for all the absorbance profiles presented in Figure 3, due to a possible presence of OH or H-C-H groups (peak (b), Fig. 3). In general, the functional groups of the significant components of the fiber are present in the spectrum of cellulose extracted from foxtail plant, verifying that the synthesis process to obtain cellulose from herbaceous material is viable. The difference differences observed in absorption spectra presented in Figure 3 may be due mainly to the extraction method, the material, and the conditions used during the experiments and sample analysis.

3.2 *Thermogravimetric analysis*

Thermogravimetric analysis (TGA) is typically used to measure thermal stability. The shape of the TGA curves generally describes mass loss as a heating function. The mass loss will vary depending on the type of cellulose particles, functional groups on the surface, heating rate, and the atmosphere (air vs. nitrogen). Figure 4 shows the corresponding TGA curves of commercial cellulose, and cellulose obtained from pink grass and foxtail plants. Commercial cellulose presents a decrease in mass at low temperatures due to water loss, followed by a significant change between 300 °C and 380 °C, which can be attributed to cellulose degradation processes such as dehydration, depolymerization, and decomposition of sugars, followed by the formation of a carbon residue (Habibi it et al., 2010).

Table 1. Wavelength absorbance regions for cellulose, hemicellulose, and lignin components obtained from plant species, reported by Raspolli Galleti *et al*., 2015; Hospodarova *et al*., 2018; Li *et al*., 2018; Javier-Astete *et al*., 2021.

Peak	Wavelength (cm^{-1})	Fiber component	Functional group	Assignment
(a)	4,000 - 2,995	Cellulose, hemicellulose and lignin	OH	Intra- and intermolecular stretching of the functional group
(b)	2,890	Cellulose, hemicellulose and lignin	CH_3 H-C-H	Symmetric methyl and methylene stretching
(c)	1,730 – 1,700	Lignin		Aromatic
(d)	1,632	Lignin	C=C	Benzene´s overlapping ring
(e)	1,640	Cellulose	Fiber-OH	OH groups bonded to fiber
(f)	1,270 - 1,108	Lignin	C-O-C C-O OH	Functional groups stretching
(g)	1,270 - 1,082	Cellulose and hemicellulose	C-O-C	Ether groups stretching

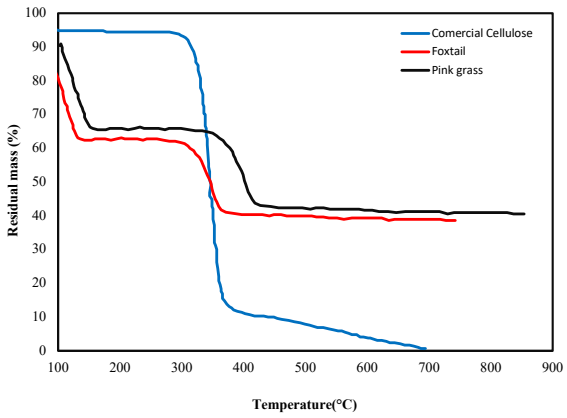

Figure 4. The graph shows TGA (Thermogravimetric Analysis) curves for the obtained samples, compared against commercial cellulose.

Further decomposition (lignin decomposition) of the residue occurs above ~425 °C, assigned to oxidation and formation of low-weight gaseous products.

The TGA curves for cellulose nanofibers obtained from foxtail plants and pink grass have a similar shape. The two curves show a decrease in mass, namely 20 % for foxtail and 10 % for pink grass, at lower temperatures than commercial cellulose. Accordingly, fibers from both plants present a notable difference; in the case of foxtail, it is between 250 °C and 380 °C, like commercial cellulose, whereas pink grass is between 300 and 420 °C. This change occurs in a broader temperature range compared to the commercial polysaccharide, which can be attributed to the increase in the content of cellulose nanofibers. Consequently, these nanomaterials present thermal stability more significant than 10% compared to cellulose. This condition can be interpreted as both samples having hydroxyl functional groups on their surfaces and between the nanofibers, which have been reported when nanocellulose is obtained by acid hydrolysis with HCl (Camarero it et al., 2013).

3.3 Morphological analysis of nanocellulose

3.3.1 High-resolution scanning electron microscopy

HR-SEM by secondary and retro-dispersed electrons was used to characterize the morphology of cellulose nanofibers at different times of physical treatment (machining). In Figure 5, samples M1 and M2 correspond to the pink grass plant at different dispersion times. The images show cellulose nanofibers with lengths greater than 1 μm but with diameters between 10 to 50 nm. This type of morphology has been commonly reported, regardless of the type of cellulose source used to obtain the nanocellulose (de Morais Teixeira it et al., 2010; Soni it et al., 2015; Ifuku it et al., 2007; Hosur it et al., 2016; Herrick it et al., 1983; Turbak it et al., 1983).

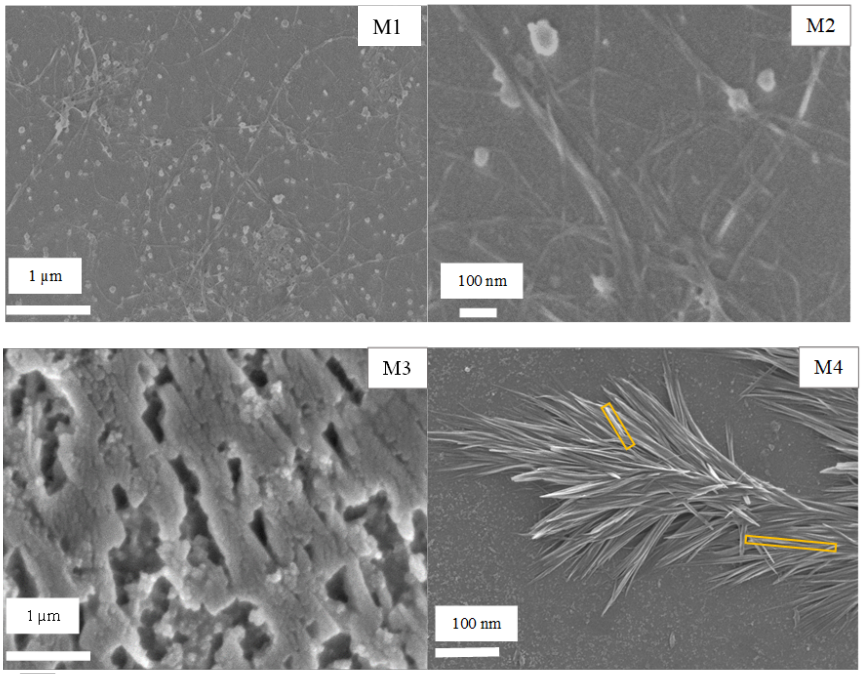

Figure 5. HR-SEM micrographs from the two plants were analyzed, showing their structure and morphology in detail. M1 (pink grass with the mechanical process to 180 min), M2 (pink grass with the mechanical process to 460 min), M3 (foxtail with the mechanical process to 180 min), and M4 (foxtail with the mechanical process to 460 min) with yellow mark are nanofibers cellulose.

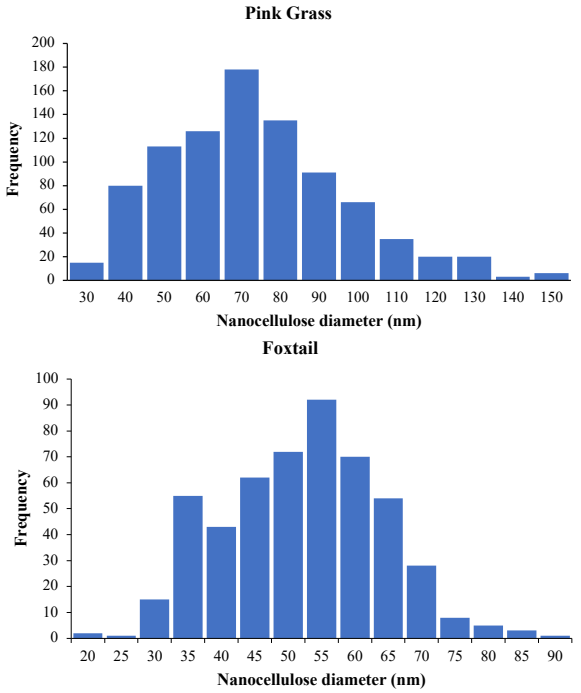

Figure 6. Particle-size distribution content for nanoparticle analysis in photomicrographs using Image J software.

Samples M3 and M4 in Figure 5 correspond to the foxtail plant. The resulting cellulose nanofibers present bouquet-like forms found as joined filaments similar to the plant's morphology at the micro-scale. Regarding the morphology and size, nanofibers in samples M3 and M4 are similar, with dimensions lower than 1 μm in length and a diameter between 50 to 80 nm. In sample M4, individual filaments are found on the bouquets. The foxtail plant presents a fractal system because the form of the cellulose nanofibers has a similar appearance to the morphology of the plant in macroscopic dimensions. This surprising result has not been reported previously.

A *fractal* is a geometric object characterized by presenting a structure that is repeated at different scales. In a way, the fractal is an endless pattern, as was proposed by Mandelbrot, and the term comes from the Latin *fractus*, which means fractured or fragmented (Mandelbrot, 2004). The fractal dimension is a relevant parameter that describes the characteristics of the fractal. This fractal dimension can also provide information about other characteristics of the nanoparticle, e.g., dynamic performance (Wang it et al., 2020). Fractal structures also give indications that the structure is very complex, as Hausdorff pointed out that one could speak of "curves" of infinite length, despite being contained in a bounded enclosure (Mauldin, 1988).

Figure 6 presents the size distribution of the fibers. In the case of nanocellulose obtained from pink grass, around 1000 nanoparticles were measured. However, carrying out measurements on the nanofibers of

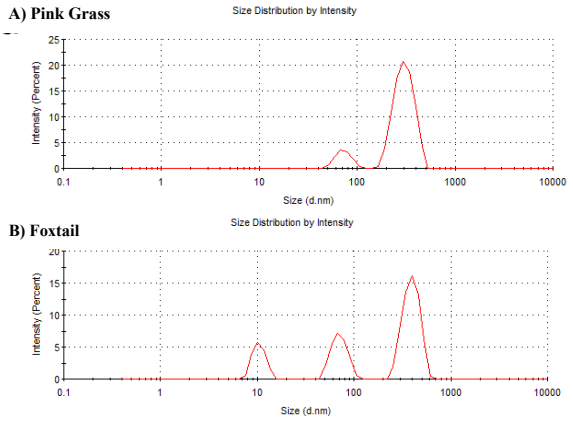

Figure 7. Particle distribution of the samples obtained by DLS.

the foxtail plant generated criteria to determine the contours of the nanofibers. In Figure 5-M4, those considered as nanofibers are indicated in yellow. In this case, it was possible to make measurements of 500 units identified as nanocellulose.

3.3.2 Dynamic light scattering

In Figure 7, the results obtained by dynamic light scattering are presented. Panel **A)** corresponds to the study on pink grass, and panel **B)** is the particle size distribution for foxtail. Former results present a bimodal distribution, with observed diameters of 51.44 nm and 295.3 nm. For the latter case, a distribution with three signals is observed, where the first peak corresponds to a particle diameter of 10.54 nm, later a diameter of 62.11 nm and 347.6 nm. Smaller diameters in both figures are those with the lowest intensity, suggesting that they are individual particles; conversely, in Figure 7 **A),** the diameter of 295.3 nm corresponds to aggregated particles.

In Figure 7 **B)**, the corresponding peaks at 62.11 nm and 347.6 nm can be identified from the length of the fibers or two-dimensional nanofiber aggregates or fractal-shaped particles. The geometry complexity of the particles was not considered in the results. Although there is a way to make comparisons between HR-SEM photomicrographs and DLS signals, in this case, it does not make sense since the nature of the nanoparticles has a very relevant impact on the particle size that DLS cannot solve. However, the analysis carried out using this optical technique allowed us to obtain information on the dispersion capacity of the system, observing that the nanofibers obtained from the foxtail plant present a more acute dispersion since the particle size distribution presents a curve with three intense peaks, at different particle sizes.

3.3.3 Transmission electron microscopy (TEM)

The images obtained by TEM allow for observing the components of the nanofibers with better resolution.

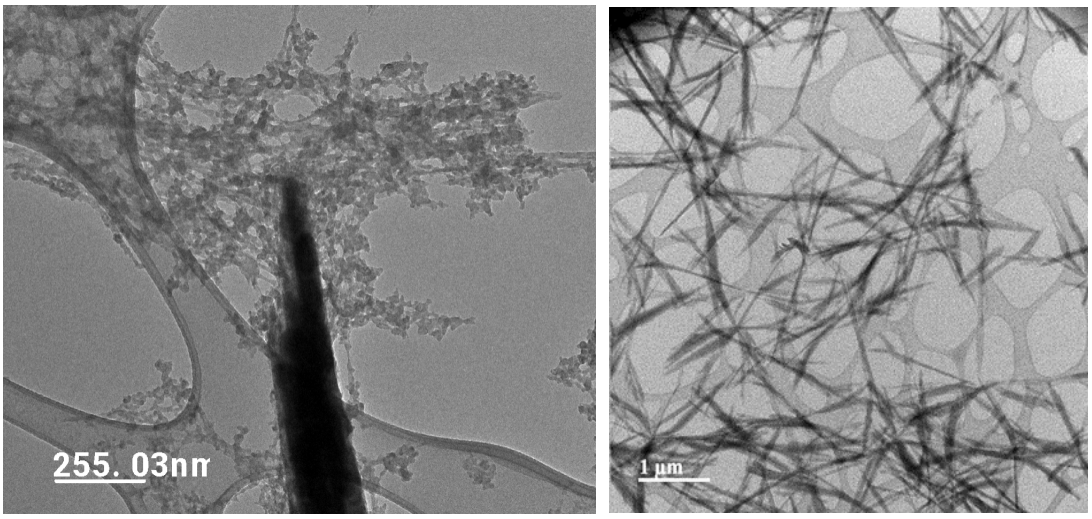

Figure 8. TEM microphotography of the nanomaterials obtained from both plants (left pink grass and right foxtail).

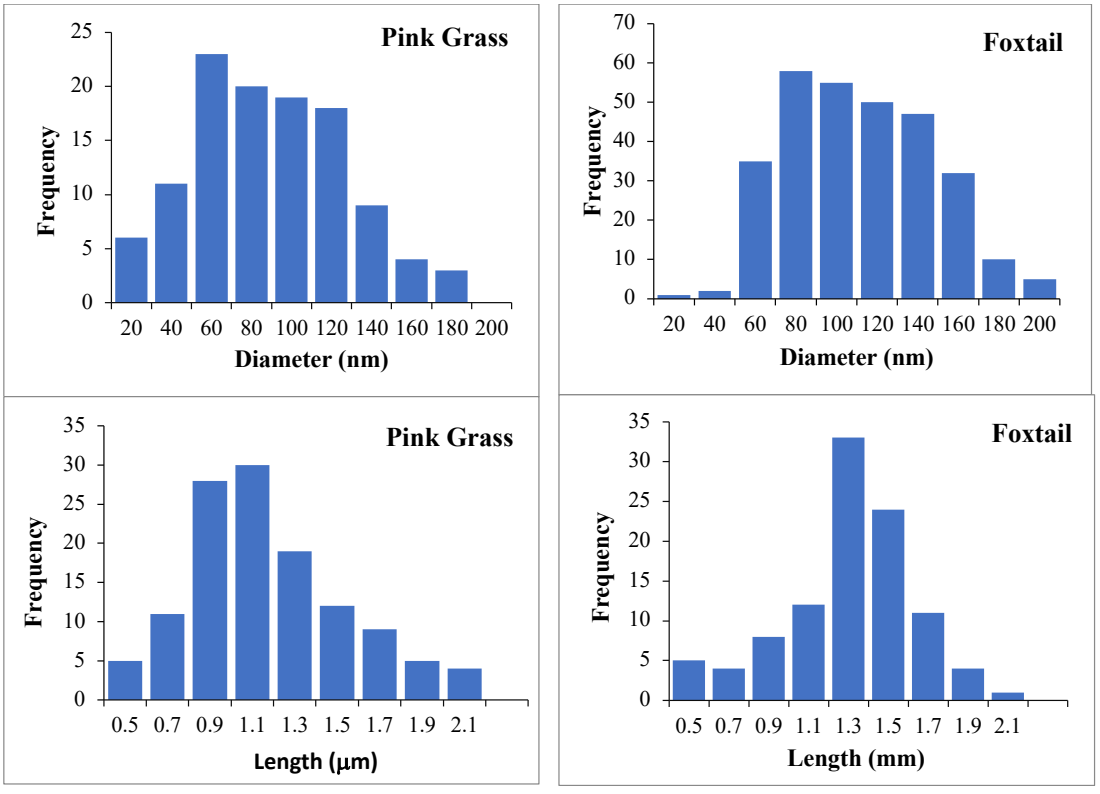

Figure 9. Diameter and length distributions obtained by TEM. Pink grass distributions on the left and foxtail plant on the right.

These images also depend on adequate sample preparation to achieve a good dispersion of the nanofibers; in this way, it is possible to perform measurements and characterize the morphology of the nanomaterials under study. Figure 8 is a TEM brightfield micrograph; on the left are the nanofibers obtained from the pink grass plant, and on the right are the nanofibers from the foxtail. The images show different nanofiber morphology for each sample.

The pink grass plant has solid-looking fibers with diameters of 60 to 200 nm, with lengths of 0.5 to 2.1 μm. The nanofibers have sharp tips, and it is impossible to observe if there are minor components at the ends of the tips. The foxtail plant sample presents a distribution of nanofibers that looks like the plant on the macro scale; this confirms what was observed in HRSEM, assuming a fractal structure.

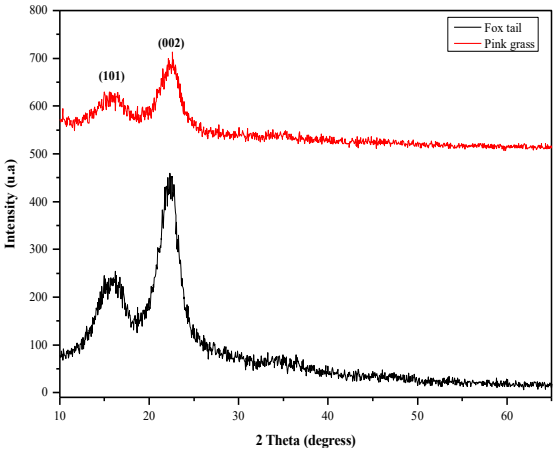

Figure 10. X-ray diffraction analysis of the nanoparticles obtained from both plants.

The foxtail tips present an appearance where the nanofiber´s minor components (ramifications) of the nanofibers can be seen, suggesting that they may be minor scaffolds of the nanofibers. The diameter sizes of these fibers range from 20 to 180 nm in diameter and 0.5 to 1.9 μm in length. The microphotographs obtained by TEM were analyzed using the Image J software generating histograms for the diameter and length of the nanofibers. The distribution of diameter and length of both plants (pink grass and foxtail plant) are shown in Figure 9. When comparing these results with those obtained by HR-SEM, it can be observed that the distributions are comparable but have a better resolution of the measurements by TEM analysis.

3.3.4 X – Rays Diffraction

The crystallinity of cellulose nanofibers is usually done by XR diffraction. According to the nature of the source of the nanocellulose, cellulose of type Iα was expected. In several reports (Segal it et al., 1959), two crystalline polymorphs are identified, and the relationship between the intensities of both does not provide information on the crystallinity of cellulose. The contribution of crystalline and disordered components constitutes the diffraction pattern. The simplest and most widely used method was developed in the 1950s by Segal it et al., 1959 and is based on the maximum height of the signals at the diffraction angles of 2θ of 22.8° and 18° representing crystalline and disordered cellulose, respectively. The results of the foxtail plant and pink grass samples show two peaks, one at 18° (disorder domain) and another at 22.8° (crystalline domain), which is the most intense in both samples (Figure 10). The crystallinity index was determined using the peak height method; the following results were obtained: pink grass = 59.43 % and for fox tail plant equal 68 %. The crystal size using Sherrer's method is 164 nm for pink grass and 126 nm for the tail plant.

Conclusion

A chemical and mechanical manufacturing process was developed to obtain cellulose nanofibers from weed plants. The chemical process was designed to remove organic matter (lignin, hemicellulose, and pectin), and in addition, this pretreatment reduces the system´s energy to facilitate obtaining cellulose nanofibers. The mechanical process replaces the chemical stage, which removes amorphous nanoparticles from the nanocellulose. This high-energy physical process uses ultrasonic radiation, at an energy of approximately 6 G, to disperse the nanoparticles with crystalline structure from the amorphous aggregates. The resulting products were characterized using different analytical techniques to confirm the quality of the cellulose nanoparticles obtained, based on comparison with reported results.

The results presented here for the sizes and morphology of nanofibers obtained from pink grass are like those reported by different authors who have obtained these nanomaterials with biomasses from different sources. However, the nanofibers obtained from the foxtail plant present a fractal-like behavior since the morphology and other structural properties are comparable at different scales.

Nanomaterials obtained from these plants showed better thermal stability than commercial cellulose in the range of 320 ºC and 700 ºC. The nanocellulose obtained from foxtail presents a higher dispersion and a narrower particle size. As for the results obtained by FTIR, the cellulose nanofibers from both plants show high levels of purity, since the characteristic bands of lignin and hemicellulose do not have a significant presence in the resulting spectra.

Acknowledgements

The authors are grateful for the support obtained from their institutions and from CONAHCYT through SNII grants. Dr. Herrera-Basurto is grateful for the CONAHCYT postdoctoral scholarship which stay was developed at CIDESI. The authors give a special recognition to Yvonne A. Joosten, MPH and Gerald G. Reed, Ph.D. for their support in the reviewing of the manuscript in English.

References

Anusiya, G., & Jaiganesh, R. (2022). A review on fabrication methods of nanofibers and a special focus on application of cellulose nanofibers. *Carbohydrate Polymer*

Technologies and Applications, 4, 100262. https://doi.org/10.1016/j.carpta.2022.100262.

Bolio-López, G.I., Valadez-González, A., Veleva, L., & Andreeva, A. (2011). Whiskers de celulosa a partir de residuos agroindustriales de banano: Obtención y caracterización. *Revista mexicana de ingeniería química*, *10*(2), 291-299. Recuperado en 07 de noviembre de 2023, http://www.scielo.org.mx/scielo.php?script=sci_arttext&pid=S1665-27382011000200013&lng=es&tlng=es

Brinchi, L., Cotana, F., Fortunati, E., & Kenny, J. (2013). Production of nanocrystalline cellulose from lignocellulosic biomass: Technology and applications. *Carbohydrate Polymers*, 94(1), 154-169. https://doi.org/10.1016/j.carbpol.2013.01.033.

Camarero Espinosa, S., Kuhnt, T., Foster, E. J., & Weder, C. (2013). Isolation of Thermally Stable Cellulose Nanocrystals by Phosphoric Acid Hydrolysis. B*iomacromolecules*, 14(4), 1223-1230. https://doi.org/10.1021/bm400219u.

Chen, Y., Fan, D., Han, Y., Lyu, S., Lu, Y., Li, G., ... & Wang, S. (2018). Effect of high residual lignin on the properties of cellulose nanofibrils/films. *Cellulose*, 25, 6421-6431. https://doi.org/10.1007/s10570-018-2006-x.

Chirayil, C. J., Mathew, L. and Thomas, S. (2014). Review of recent research in nano cellulose preparation from different lignocellulosic fibers. *Rev. Adv. Mater. Sci*., vol. 37, no. 1–2, pp. 20–28.

Djafari Petroudy, S. R., Chabot, B., Loranger, E., Naebe, M., Shojaeiarani, J., Gharehkhani, S., Ahvazi, B., Hu, J., & Thomas, S. (2021). Recent advances in cellulose nanofibers preparation through energy-efficient approaches: A review. *Energies*, 14(20), 6792. https://doi.org/10.3390/en14206792.

De Morais Teixeira, E., A. C. Corrêa, A. Manzoli, F. de Lima Leite, C. de Ribeiro Oliveira, and L. H. C. Mattoso. (2010), Cellulose nanofibers from white and naturally colored cotton fibers. C*ellulose*, 17, 3, 595–606. https://doi.org/10.1007/s10570-010-9403-0.

Dufresne, A. (2013). Nanocellulose: a new ageless bionanomaterial. *Materials Today*, 16(6), 220-227. https://doi.org/10.1016/j.mattod.2013.06.004.

Finch, C. A. (1985). Cellulose chemistry and its applications. *British Polymer Journal*, 17(3), 552. https://doi.org/10.1002/pi.4980170313.

Fleming, K., Gray, D. G., Matthews, S. (2001). Cellulose crystallites. *Chemistry- A European Journal*, 7(9), 1831-1836. https://doi.org/10.1002/1521-3765(20010504)7:9%3c1831::AID-CHEM1831%3e3.0.CO;2-S.

French, A. D., Pérez, S., Bulone, V., Rosenau, T. (2002). Encyclopedia of Polymer Science and Technology. *Cellulose.* 1838. https://doi.org/10.1002/0471440264.pst042.pub2

Gardner, K. H., & Blackwell, J. (2001). The structure of native cellulose. *Biopolymers*, 13(10), 1975-2001. https://doi.org/10.1002/bip.1974.360131005.

Garzón, M. de L., Tecante, A., Ramírez-Gilly, M., & Palacios, J. (2009). Comportamiento viscoelástico de disoluciones y tabletas hidratadas de hidroxipropilmetil celulosa, carboximetil celulosa sódica y sus mezclas. *Rev. Mex. Ing. Quim.*, *8*(3), 307-318.

Habibi, Y., Lucia, L. A., & Rojas, O. J. (2010). Cellulose Nanocrystals: Chemistry, Self-Assembly, and Applications. *Chemical Reviews*, 110(6), 3479-3500. https://doi.org/10.1021/cr900339w.

Herrick, F. W., Casebier, R. L., Hamilton, J. K., and Sandberg, K. R. (1983). Microfibrillated cellulose: morphology and accessibility. United States.

Hospodarova, V., Singovszka, E., and Stevulova, N. (2018). Characterization of Cellulosic Fibers by FTIR Spectroscopy for Their Further Implementation to Building Materials. *American Journal of Analytical Chemistry*, 9, 303-310. https://doi.org/10.4236/ajac.2018.96023.

Hosur, M., Baah, D., Nuruddin, M., Jamal Uddin, M. and Jeelani, S. (2016). A novel approach for extracting cellulose nanofibers from lignocellulosic biomass by ball milling combined with chemical treatment. Wiley Online Libr. 133, 9, 42990.

Ifuku, S., Nogi, M., Abe, K., Handa, K. Nakatsubo, F. and Yano, H. (2007). Surface modification of bacterial cellulose nanofibers for property enhancement of optically transparent composites: dependence on acetyl-group DS. *Biomacromolecules,* 8(6), 1973–1978. https://doi.org/10.1021/bm070113b.

Ioelovich, M. (2008). Cellulose as a nanostructured polymer: A short review. *BioResources*, 3(4), 1403-1418. https://doi.org/10.15376/biores.3.4.ioelovich.

Isogai, A. (2020). Cellulose nanofibers: Recent progress and future prospects. *Journal of Fiber Science and Technology*, 76(10), 310-326. https://doi.org/10.2115/fiberst.2020-0039.

Javier-Astete, R., Jimenez-Davalos, J., Zolla, G. (2021). Determination of hemicellulose, cellulose, holocellulose and lignin content using FTIR in *Calycophyllum spruceanum* (Benth.) K. Schum. and *Guazuma crinita* Lam. *PLoS ONE* 16, e0256559. https://doi.org/10.1371/journal.pone.0256559.

Khalid, M. Y., Al Rashid, A., Arif, Z. U., Ahmed, W., & Arshad, H. (2021). Recent advances in nanocellulose-based different biomaterials: types, properties, and emerging applications. *Journal of Materials Research and Technology,* 14, 2601-2623. https://doi.org/10.1016/j.jmrt.2021.07.128.

Li, X., Wei, Y., Xu, J., Xu, N., and He, Y. (2018). Quantitative visualization of lignocellulose components in transverse sections of moso bamboo based on FTIR macro- and micro-spectroscopy coupled with chemometrics. Biotechnology for Biofuels, 11, 263. https://doi.org/10.1186/s13068-018-1251-4.

Ltd, R. A. M. (s. f.). Global Nanocellulose Market - Forecast to 2030. Research and Markets ltd 2023. https://www.researchandmarkets.com/reports/5009171/global-nanocellulose-market-by-type-mfc-and-nfc [Accessed: 10-Apr-2023].

Mandelbrot, Benoit B. (2004). Fractals and Chaos: the Mandelbrot set and beyond (Vol. 3), New York: Springer. (2004).

Marchessault, R.H. (1962). Application of infra-red spectroscopy to cellulose and wood polysaccharides. *Pure and Applied Chemistry*, 5, 107 - 130.

Mauldin, R. D. and S. C., Williams. (1988). Hausdorff dimension in graph directed constructions, *Transactions of the American Mathematical Society*, 309(2), 811-829. https://doi.org/10.2307/2000940.

Nair, S. S., Zhu, J. Y., Deng, Y., & Ragauskas, A. J. (2014). Characterization of cellulose nanofibrillation by micro grinding. *Journal of Nanoparticle Research*, 16(4). https://doi.org/10.1007/s11051-014-2349-7.

Ponce-Reyes, C. E., Chanona-Pérez, J. J., Garibay-Febles, V., Palacios-González, E., Karamath, J., Terrés-Rojas, E., & Calderón-Domínguez, G. (2014). Preparation of cellulose nanoparticles from agave waste and its morphological and structural characterization. *Revista Mexicana de Ingeniería Química*, *13*(3), 897–906. https://www.scielo.org.mx/pdf/rmiq/v13n3/v13n3a21.pdf.

Postek, M., Moon, R., Rudie, A. and Bilodeau, M. (2013) "Production and applications of cellulose". Tappi Press. Peachtree Corners.

Raspolli Galleti, A. M., D'Alessio, A., Licursi, D., Antonetti, C., Valentini, G., Galia, A., and Nassi o Di Nasso, N. (2015). Midinfrared FT-IR as a Tool for Monitoring Herbaceous Biomass Composition and Its Conversion to Furfural. *Journal of Spectroscopy*, 2015, 1-12. https://doi.org/10.1155/2015/719042.

Ruiz-Palomero, C., Soriano, M. L., & Valcárcel, M. (2017). Nanocellulose as analyte and analytical tool: Opportunities and challenges. *TrAC Trends in Analytical Chemistry*, 87, 1-18. https://doi.org/10.1016/j.trac.2016.11.007.

Segal, L., Creely, J. J., Martin, A. E. and Conrad, C. M. (1959). An empirical method for estimating the degree of crystallinity of native cellulose using the x-ray diffractometer, Text. Res., 29, 786-794.

Shaghaleh, H., Xu, X., & Wang, S. (2018). Current progress in production of biopolymeric materials based on cellulose, cellulose nanofibers, and cellulose derivatives. *RSC advances*, 8(2), 825-842. https://doi.org/10.1039/C7RA11157F.

Soni, B., Hassan, E. B., & Mahmoud, B. (2015). Chemical isolation and characterization of different cellulose nanofibers from cotton stalks. *Carbohydrate Polymers*, 134, 581-589. https://doi.org/10.1016/j.carbpol.2015.08.031.

Thomas, P., Duolikun, T., Rumjit, N. P., Moosavi, S., Lai, C. W., Bin Johan, M. R., & Fen, L. B. (2020). Comprehensive review on nanocellulose: Recent developments, challenges and future prospects. *Journal of the Mechanical Behavior of Biomedical Materials*, 110, 103884. https://doi.org/10.1016/j.jmbbm.2020.103884.

Trache, D., Tarchoun, A. F., Derradji, M., Hamidon, T. S., Masruchin, N., Brosse, N., & Hussin, M. H. (2020). Nanocellulose: From Fundamentals to Advanced Applications. *Frontiers in Chemistry*, 8. https://doi.org/10.3389/fchem.2020.00392.

Turbak, A F, Snyder, F W, and Sandberg, K R. (1983). Microfibrillated cellulose, a new cellulose product: properties, uses, and commercial potential. United States.

Wang, X., Song, Z., Gao, Q., and Song, R. (2020). Study on the fractal structure of carbon nanomaterials' smokescreen. In IOP Conference Series: Materials Science and Engineering, Vol. 892, No. 1, p. 012010. https://10.1088/1757-899X/892/1/012010.

Winter, A., Andorfer, L., Herzele, S., Zimmermann, T., Saake, B., Edler, M., Griesser, T., Konnerth, J., & Gindl-Altmutter, W. (2017). Reduced polarity and improved dispersion of microfibrillated cellulose in poly (lactic-acid) provided by residual lignin and hemicellulose. *Journal of materials science*, 52, 60-72. https://doi.org/10.1007/s10853-016-0439-x.